

Electric Ion Dispersion as a New Type of Mass Spectrometer

Michael Lindstrom ^{*}; Iain Moyles [†]; Kevin Ryczko [‡]

October 29, 2014

Abstract

At the 2014 Fields-MPrime Industrial Problem Solving Workshop, PerkinElmer presented a design problem for mass spectrometry. Traditionally mass spectrometry is done via three methods: using magnetic fields to deflect charged particles whereby different masses bend differently; using a time-of-flight procedure where particles of different mass arrive at different times at a target; and using an electric quadrupole that filters out all masses except for one very narrow band. The challenge posed in the problem was to come up with a new design for mass spectrometry that did not involve magnetic fields and where mass-fractions could be measured in an entire sample on a continuous basis. We found that by sending the sample particles down a channel of line charges that oscillations would be induced with a spatial wave-length being mass-dependent thereby allowing different masses to be separated spatially and potentially detected on a continuous basis, without the use of magnetic fields. In this paper, we present the analysis of our design and illustrate how this principle could be used for mass spectrometry.

keywords: mass spectrometry, electric fields, mass dispersion, harmonic motion

1 Background

1.1 Mass Spectrometry

Mass spectrometry is a technique used to determine the chemical composition of a certain substance or substances by separating atomic elements by mass. The most common underlying mechanism of most mass spectrometers is by ionizing each particle, giving each particle the same net positive charge and exploiting their mass-charge ratio. There are three mechanisms that are primarily used for industrial mass spectrometers [4]. One technique uses

^{*}Institute for Applied Math, University of British Columbia mlrtlm@math.ubc.ca

[†]Institute for Applied Math, University of British Columbia imoyles@math.ubc.ca

[‡]Department of Physics, University of Ontario Institute of Technology kevin.ryczko@uoit.net

magnetic fields to separate masses into rings of distinct radii which can then be detected. The use of magnetic fields however is quite costly and was not desired by our industrial partner. The second most common technique is a procedure known as time of flight which excites the mass sample by giving it kinetic energy and sending the particles through a given path. Because the particles will have different accelerations, this makes all the particles have different velocities and hence for a fixed detector position, they will have different travel times. It was indicated to us by the industrial partner however that this method is also not desirable because the kinetic excitation comes in pulses of energy which means that any transient changes in chemical composition will not be detected. With these considerations in mind, it was desired by the industrial sponsor to design a mass spectrometer that only uses electric fields and that doesn't lose any sample resolution. It was also noted that devices that "trap" particles, confining them to localized spatial regions for later detection, are less desirable as this again does not allow for continuous measurement of composition.

Another device that is used is known as a Quadrupole Mass Spectrometer (cf. [4], [2], [5]) which works as a bandpass filter separating masses. The design has 4 conductors which have a base DC voltage plus an AC voltage such that diametrically opposite electrodes have the same potential and adjacent electrodes have opposite voltages. The AC voltage is such that heavy masses do not react to the changing polarity fast enough, effectively only feeling the base DC and hence slowly drifting to the conductor that was originally negatively charged and eventually annihilating. This is the low pass component of the filter. Conversely, the lighter positive charges feel the effect of the modulating AC and doesn't notice the DC. Very light charged particles are impacted by the AC very quickly, being excited due to resonance effects [5] and thereby collide with the electrodes near entry. This is the high pass filter component of the device. With these effects combined, parameters can be chosen to isolate a band of a single mass to pass through the detector. In order to detect several masses, industrialists need to inject repeated copies of the sample and adjust parameters to change the isolated mass. While the industrial partner was generally happy with this device, they were concerned about the time taken to process individual masses as well as the potentially limited amount of initial sample available. In this paper, we explore the task of finding a device that could detect multiple masses at once keeping these stipulations in mind.

1.2 Electric Ion Dispersion

Our idea presented in this paper is based on harmonic oscillation. If two fixed positive point charges were separated and a positive charge were introduced at a point away from the equilibrium of the charges, oscillations about the equilibrium would occur in a one-dimensional system. The period of these oscillations will be mass dependent. Likewise, if the charged particles were deflected from the edges of a long device and all maintained a roughly constant axial velocity, the temporal periods will translate into spatial wavelengths whereby different masses have different wavelengths. Such a property could be exploited to induce a mass dispersion. See Figure 1. Note that we consider a series of isolated point-charges instead of a line of charge. In the limit, as we show, this point-charge model reduces to a line-charge model. It is potentially more practical from an engineering perspective to

have isolated charges insulated from each other than line charges. By analyzing the model with these isolated charges, we in effect analyze the line charge model as well. Observe that this device operates in a plane. While it may seem natural to extend this to a solenoidal geometry, as we observe in our modelling work, a solenoid approximates a cylinder with constant boundary potential too well and thus the desired effect is not achieved as the net electric field inside is approximately zero.

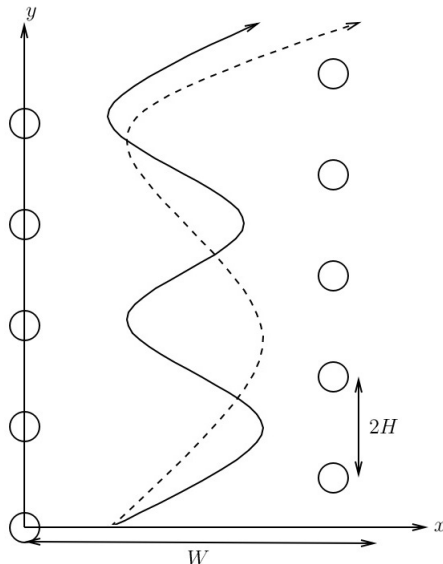


Figure 1: A sketch of the line charge device: within the plane, particles enter from the bottom and are excited into oscillations in x with approximately constant y -velocity. The circles indicate positive charges of charge $+Ze$ with a vertical spacing of $2H$. In the implementation, likely H would be very small so that particles cannot exit through the sides of the device, or if practical the isolated charges could be replaced by a line of charges with uniform linear charge density.

2 Designs

We consider two designs here. The first design illustrates a proof-of-principle for our ion dispersion technique and is two-dimensional, with the sides consisting of isolated charges along a line. This model will be amenable to mathematical analysis. The second design is less straightforward to analyze and we rely upon numerical methods. It consists of a helical wire carrying a uniform linear charge density. It is unfortunately not useful in producing the desired mass dispersion effects. All of our analysis is based on simple principles of non-relativistic electrostatics, for which [3] is an excellent reference.

2.1 Line Charges Design

Charges with net charge Ze are placed along the line $x = 0$ at positions $y = 0, 2H, 4H, 6H, \dots$ and at positions $x = H, 3H, 5H, 7H, \dots$. The staggering adds an extra level of protection that the moving particles don't escape through the sides of the device. Any charges that are placed in the dispersion device will experience forces from the fixed point charges along the device via Coulomb's Law:

$$V = \frac{Ze}{4\pi\epsilon_0} \sum_{j=1}^N \left(\frac{1}{\sqrt{x^2 + (y - 2jH)^2}} + \frac{1}{\sqrt{(x - 1)^2 + (y - (2j - 1)H)^2}} \right),$$

$$m\ddot{\mathbf{x}} = -e\nabla V$$

where we neglect particle-particle interactions at this point. Here, e is the fundamental electric charge, Z is the charge number for the fixed point charges on the device, N is the half the number of device charges on each side of the device, H is the half the vertical spacing between adjacent charges (due to the non-symmetric staggered charge distribution across the two sides of the device), and ϵ_0 is the permeativity of free space, and m is the mass of the entering test charge. We make the following non-dimensionalizations:

$$x = W\bar{x}, \quad y = W\bar{y}, \quad t = \frac{W}{U_0}\bar{t}$$

where W is the width of the device and U_0 is the magnitude of a typical incoming particle velocity, i.e.

$$U_0 = \sqrt{U_{0x}^2 + U_{0y}^2}.$$

If we define the following quantities

$$h = \frac{H}{W},$$

$$\beta_m = \frac{Ze^2 m_p / m}{4\pi\epsilon_0 m_p W U_0^2},$$

$$\bar{r}_j = \sqrt{\bar{x}^2 + (\bar{y} - 2jh)^2},$$

$$\bar{\rho}_j = \sqrt{(\bar{x} - 1)^2 + (\bar{y} - (2j - 1)h)^2}$$

then we can write our non-dimensional system as (dropping the overbars for convenience):

$$\ddot{x} = \beta_m \sum_{j=1}^N \left(\frac{x}{r_j^3} + \frac{x - 1}{\rho_j^3} \right), \tag{1a}$$

$$\ddot{y} = \beta_m \sum_{j=1}^N \left(\frac{y - 2jh}{r_j^3} + \frac{y - (2j - 1)h}{\rho_j^3} \right). \tag{1b}$$

All parameter values are listed in Table 1.

Parameter	Description	Value
W	Width of Device	0.1m
H	Half Charge Spacing on Device	1×10^{-4} m
U_0	Incoming Particle Velocity	$\sqrt{2} \times 10^4$ ms ⁻¹
e	Elementary Charge Constant	1.6×10^{-19} C
Z	Charge Number of Device Charges	15
N	Quantity of Device Charges on Each Side of Device	20000
ϵ_0	Permeativity of Free Space	8.85×10^{-12} CV ⁻¹ m ⁻¹
m_p	Mass of a Proton	1.6726×10^{-27} kg

Table 1: Parameters used in non-dimensional model of ion dispersion.

2.2 Solenoidal Design

We consider a solenoidal geometry with a wire of uniform charge density parameterized as a helical segment. Our wire takes the form

$$\langle x(\theta), y(\theta), z(\theta) \rangle = \langle R_0 \cos(\theta), R_0 \sin(\theta), \alpha R_0 \theta \rangle$$

with $0 \leq \theta \leq \frac{2NH}{R_0\alpha}$, carrying a uniform charge density

$$\lambda = \frac{Ze}{2\pi R_0 \sqrt{1 + \alpha^2}}.$$

By setting $R_0 = W/2$, this solenoid has the same width as the separated charges and with

$$\alpha = \frac{H}{2\pi R_0},$$

the spacing between charges in the separated charge design corresponds to the z -distance between consecutive helical rings. Also, for every change of θ by 2π , the wire length is $2\pi R_0 \sqrt{1 + \alpha^2}$ giving a total charge of Ze . With this, the potential energy of a particle of charge e is

$$V = \frac{R_0 \lambda \sqrt{1 + \alpha^2} e}{4\pi \epsilon_0} \int_0^{\frac{2NH}{R_0\alpha}} \frac{d\theta}{\sqrt{(x - R_0 \cos \theta)^2 + (y - R_0 \sin \theta)^2 + (z - R_0 \alpha \theta)^2}}.$$

This integral is obtained by integrating the potential energy contribution of each differential arc length element of the helix over the length of the helix.

We then make the nondimensionalizations:

$$\langle x, y, z \rangle = R_0 \langle \bar{x}, \bar{y}, \bar{z} \rangle, \quad t = \frac{R_0}{U_0} \bar{t}$$

and define

$$\gamma_m = \frac{Ze^2 m / m_p}{8\pi^2 \epsilon_0 m_p R_0 U_0^2 \sqrt{1 + \frac{H^2}{4\pi^2 R_0^2}}}.$$

In dimensionless form the equations of motion $m \frac{d^2}{dt^2} \langle x, y, z \rangle = -\nabla V$, again dropping the overbars can be expressed by:

$$\langle \ddot{x}, \ddot{y}, \ddot{z} \rangle = \gamma_m \int_0^{\frac{2NH}{R_0\alpha}} \frac{\langle \cos \theta - x, \sin \theta - y, \alpha\theta - z \rangle}{((x - \cos \theta)^2 + (y - \sin \theta)^2 + (z - \alpha\theta)^2)^{3/2}} d\theta \quad (2)$$

2.3 Initializations

2.3.1 Design Initial Conditions

Given $x = y = 0$ is the bottom-left corner of the line charge device then in order to have incoming particles enter from outside the device we require

$$y(0) = y_0 < 0.$$

It was previously mentioned that the premise of the device is oscillation around the equilibrium of point charges. This equilibrium lies directly at the center of the device and therefore, in order to have periodic motion we take,

$$x(0) = x_0, \quad 0 < x_0 < \frac{1}{2}.$$

Without loss of generality, we can set

$$\dot{x}(0) = 0$$

because by placing the particle away from equilibrium with respect to the device charges, we will induce horizontal motion for $t > 0$. Imposing the initial vertical velocity is slightly less straight-forward. If the velocity is too high then the particles will enter and exit the device before any effective horizontal motion can begin. Conversely, if the charge is too small then the incoming particle will be repelled by the charges in front of it and will not have enough energy to enter the device. We therefore need the velocity to be sufficient to overcome the initial potential barrier but to not be too large. To approximate the potential barrier, we consider a ‘‘centre of charge’’ argument where all of the wall charges are concentrated as a single charge in the centre of the device. If this were the case, we want to give the particle enough kinetic energy to overcome the potential difference of its relative starting position to this group charge and the distance between the particle and the group charge at the entry of the device. With this in mind we get the following inequality for the vertical velocity,

$$\dot{y}(0) > \sqrt{\frac{Z\beta_m N}{\left(\left(x_0 - \frac{1}{2}\right)^2 + (Nh)^2\right)^{1/2}} - \frac{Z\beta_m N}{\left(\left(x_0 - \frac{1}{2}\right)^2 + (y_0 - Nh)^2\right)^{1/2}}}.$$

Using the values $x_0 = 1/4$ and $y_0 = -1$ along with the parameters in Table 1, we get that

$$\dot{y}(0) \gtrsim 0.1,$$

i.e. the initial velocity has to be at least 10% of the dimensional U_0 velocity. According to our industrial partner, this velocity is easy to achieve for any initial concentration.

Our argument for the initialization of the solenoidal design is identical: the particles are fired into the device away from the central axis.

3 Numerical Results

We implemented numerical and analytical techniques to analyze the designs.

3.1 Line Charge Design

We implemented the model using `ode45` in Matlab choosing parameters from Table 1 and taking $x(0) = 1/4$, $y(0) = -1$, $\dot{x}(0) = 0$, and $\dot{y}(0) = 0.2$. Figure 2 shows the $x-y$ trajectories for a series of masses ($0.5m_p$, m_p , and $2m_p$) with the blue curve being the trajectory for mass $0.5m$, the black curve for mass m and the red curve for mass $2m$. The spacing between charges is non-dimensionally h and so the length of the device is $2Nh$.

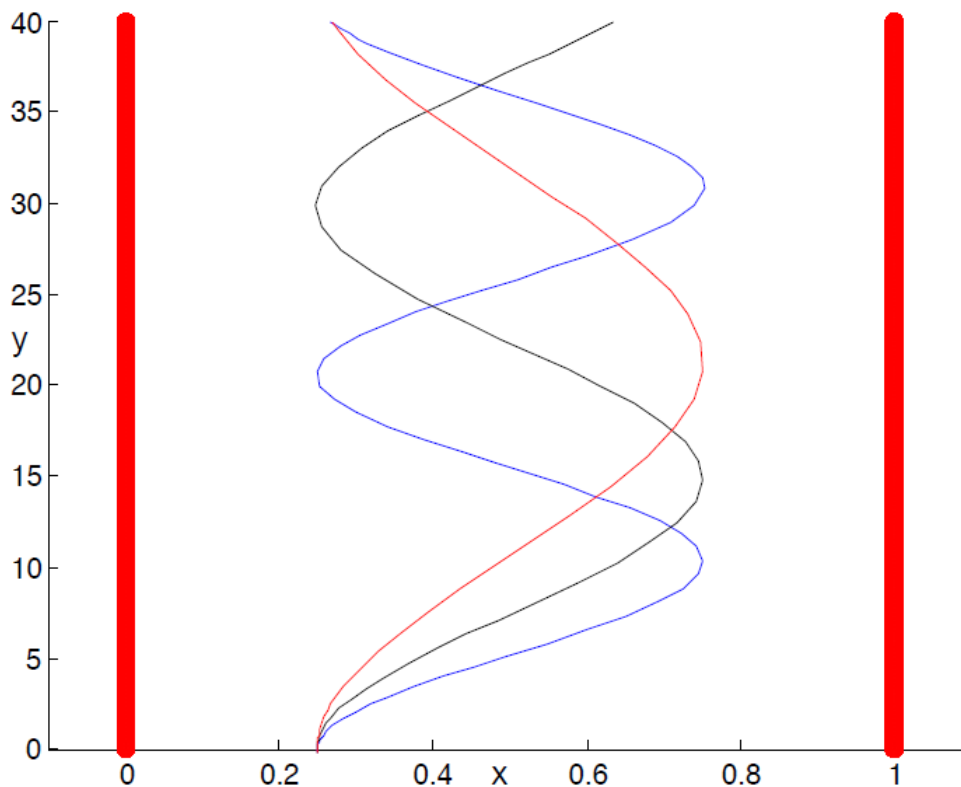


Figure 2: The red lines along the side represent the small spaced point charges while the curves inside are the trajectories of different masses. The blue curve is the trajectory for the mass $0.5m$, the black curve is the trajectory for mass m , and the red curve is the trajectory for mass $2m$.

Very quickly, we see that the mass dispersion relation has separated the three particles. Figure 3 shows the y -velocity for the mass m .

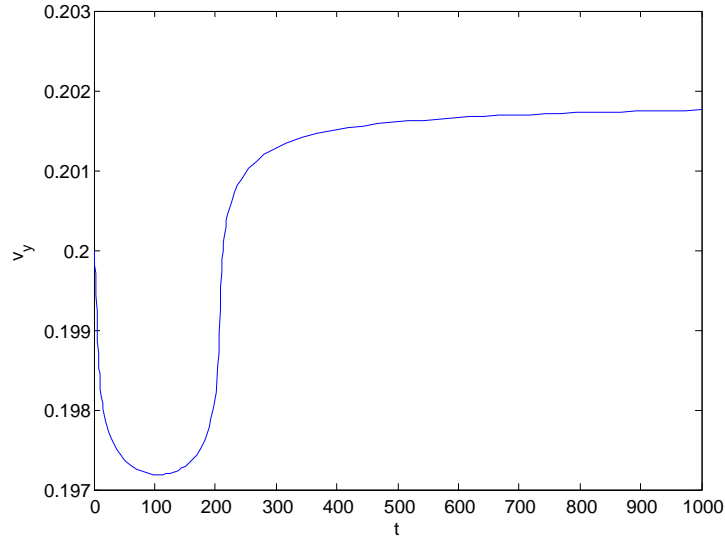


Figure 3: Plot of y -velocity over time. The “sharp” transition regions are where the particles enter and exit the device respectively separating two regions of essentially constant velocity. The transition regions themselves experience a very small acceleration.

While there is a vertical acceleration through the device, it is quite small. This effect is seen in any mass that enters the device with smaller masses having the larger accelerations. Therefore, the device appears to have the original intention of maintaining y -velocity and reducing the problem to that of a single oscillator between two charges. In the sections that follow, comparisons with numerics refer to plots generated using this `ode45` implementation.

3.2 A Posteriori Justification of Negligible Interaction Forces

Although we neglected the interaction between individual charged particles in the numerical results, focusing solely upon the forces induced by the charged cavity on the particles, we justify the negligible forces by considering how big the force between two particles would be if they traveled along their natural trajectories $(x_1(t), y_1(t))$ and $(x_2(t), y_2(t))$ by considering only the forces induced by the charged walls. We consider two particles of dimensionless mass $1m_p$ and $2m_p$, originating at $(1/4, -1)$ with zero initial x -velocity and a y -velocity of 0.2 and plot the force

$$f(t) = \frac{\tilde{\beta}_m m / m_p}{(x_1(t) - x_2(t))^2 + (y_1(t) - y_2(t))^2}$$

versus time, both in dimensionless units, when both particles have entered the device. Note that $\tilde{\beta}_m = \beta_m / 15$ because the charge of the individual particles are $Z = e$ and not $Z = 15e$. We also can compute the dimensionless force of the device acting on the particles over that same range of time via

$$f_j(t) = a_j(t) / \beta_m$$

where $a_j(t)$ is the magnitude of the dimensionless acceleration of particle j .

As we observe in figures 4 and 5, the dimensionless force exerted on the particles by the device greatly exceeds the force exerted between the two particles on each other by several orders of magnitude. The smallest force exerted on the particles by the device is still roughly 60 and generally much larger, whereas the typical scale of the force between the two particles is 1×10^{-4} . The plots of the forces are for two particles, but even for hundreds, the forces between particles would be negligible. Particle collisions are another possibility, but these tend to be very infrequent and the main effect would be to reduce the particle velocities as noted in [1].

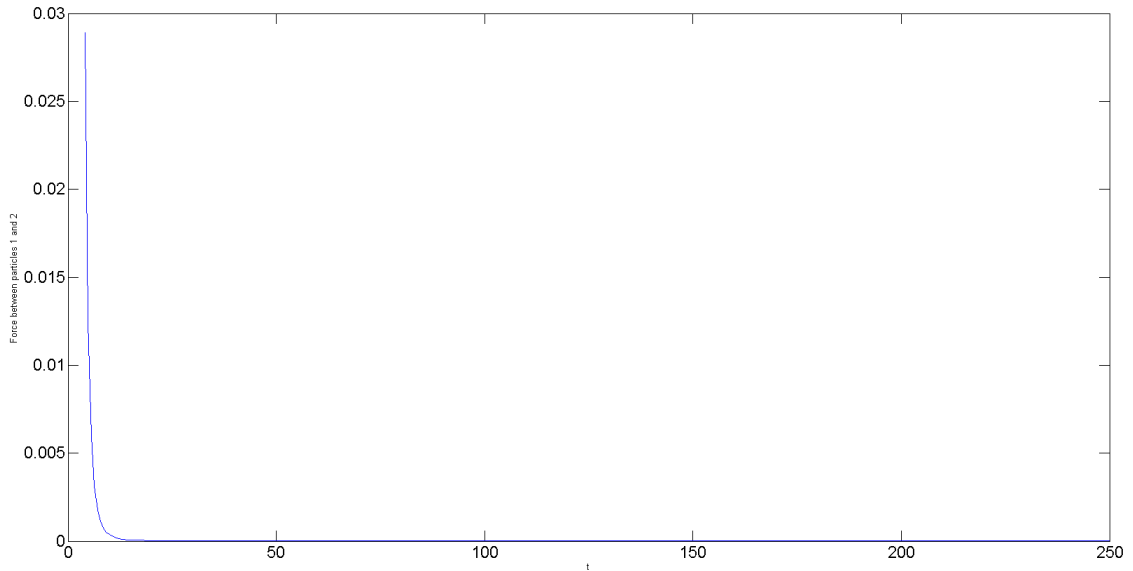


Figure 4: The dimensionless force between the two particles of mass m_p and $2m_p$ as they move along their trajectories.

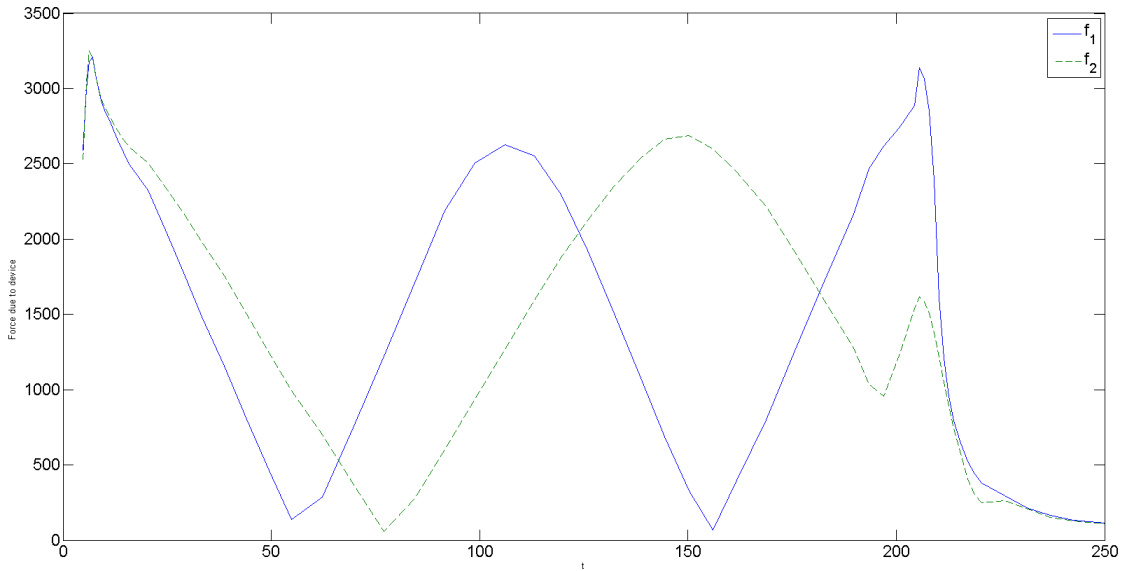


Figure 5: The dimensionless force exerted by the device on the particles of mass m_p and $2m_p$ denoted by f_1 and f_2 respectively.

3.3 Solenoidal Design

We include a plot of a trajectory found in the solenoidal model in figure 6. With the solenoid, there is minimal bending and, although not evident from the plot, there is a nearly constant drift of the ionized particles within the device instead of a helix as desired. We attribute this to the fact that when the helix is tightly coiled (as is necessary to reduce the risk of particles leaving the device through its sides) then a uniform voltage on the helical walls very closely approximates a constant potential on the walls of a cylinder whereby the inner electric field is zero and thus particles drift but are not accelerated.

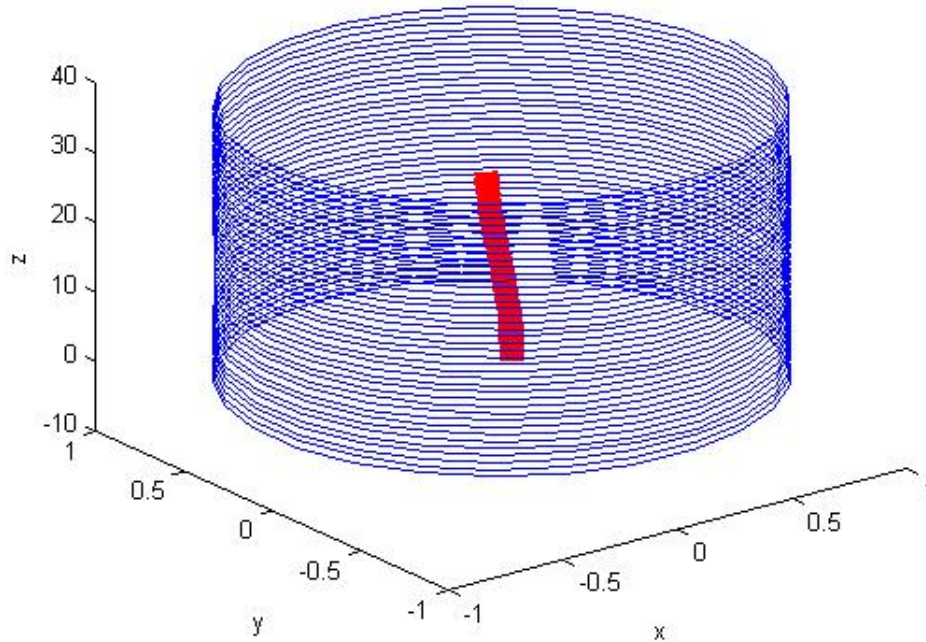


Figure 6: This plot shows the trajectory of the charged particles (red) entering through the device (blue) at $z = 0$. Note there is a slight deflection but ultimately there is only a drift.

4 Analytic Results

Since N , the number of charges on each side of the device, is so large in the staggered charge model, we expect that the summation in equation (1) can be replaced by an integral. Indeed this is how a line charge model can be derived by taking a limit of point-charges. The device sides in Figure 2 are discrete charges but appear as a single line charge when the spacing is very small. Performing a Riemann summation, we can approximate the following sums as integrals:

$$\beta \sum_{j=1}^N \frac{x}{r_j^3} \approx -\frac{\beta}{2h} \int_y^{y-2Nh} \frac{x}{(x^2 + s^2)^{3/2}} ds$$

$$\beta \sum_{j=1}^N \frac{y - 2jh}{r_j^3} \approx -\frac{\beta}{2h} \int_y^{y-2Nh} \frac{t}{(x^2 + q^2)^{3/2}} dq.$$

Similar integration transformations follow for the ρ_j summations. Using these integrals as replacements in (1) and performing the integration we get a new line-charge continuum

model:

$$\ddot{x} = -\frac{\beta}{2hx} \left(\frac{y-2Nh}{\rho_{x,y-2Nh}} - \frac{y}{\rho_{x,y}} \right) - \frac{\beta}{2h(x-1)} \left(\frac{y-2Nh}{\rho_{x-1,y-2Nh}} - \frac{y}{\rho_{x-1,y}} \right) \quad (3a)$$

$$\ddot{y} = -\frac{\beta}{2h} \left(\frac{1}{\rho_{x,y}} - \frac{1}{\rho_{x,y-2Nh}} + \frac{1}{\rho_{x-1,y}} - \frac{1}{\rho_{x-1,y-2Nh}} \right) \quad (3b)$$

where

$$\rho_{a,b} = \sqrt{(x-a)^2 + (y-b)^2}.$$

Solving (3) numerically using `ode45` and comparing it to the numeric computations of (1) for a single mass m is displayed in Figure 7 which shows relatively strong agreement.

In the design of interest, the length $L = 2Nh \gg 1$ and we can exploit this to obtain a leading-order asymptotic estimate for the accelerations given in equations (3a) and (3b) when $0 < x < 1$ and $y = L/2 + u$ with $|u| \ll L$ i.e. when the particles are well into the device with respect to either end. In essence we are performing an asymptotic expansion in the acceleration equations starting at some time when $y \approx Nh$. We write

$$\begin{aligned} \ddot{x} &= -\frac{\beta}{2hx} \left(\frac{u-L/2}{\sqrt{x^2 + (u-L/2)^2}} - \frac{L/2+u}{\sqrt{x^2 + (u+L/2)^2}} \right) \\ &\quad - \frac{\beta}{2h(x-1)} \left(\frac{u-L/2}{\sqrt{(x-1)^2 + (u-L/2)^2}} - \frac{y}{\sqrt{(x-1)^2 + (u+L/2)^2}} \right) \\ &= -\frac{\beta}{2hx} \left(\frac{-L/2 + o(L)}{\sqrt{L^2/4 + O(L)}} - \frac{L/2 + o(L)}{\sqrt{L^2/4 + O(L)}} \right) - \frac{\beta}{2h(x-1)} \left(\frac{-L/2 + o(L)}{\sqrt{L^2/4 + O(L)}} - \frac{L/2 + o(L)}{\sqrt{L^2/4 + O(L)}} \right) \\ &\sim \frac{-\beta}{hx} + \frac{\beta}{h(x-1)} + o(1) \quad \text{and} \\ \ddot{y} &= -\frac{\beta}{2h} \left(\frac{1}{\sqrt{x^2 + (L/2+u)^2}} - \frac{1}{\sqrt{x^2 + (u-L/2)^2}} + \frac{1}{\sqrt{(x-1)^2 + (L/2+u)^2}} - \frac{1}{\sqrt{(x-1)^2 + (u-L/2)^2}} \right) \\ &= -\frac{\beta}{2h} \left(\frac{2}{L} - \frac{2}{L} + \frac{2}{L} - \frac{2}{L} \right) + o(1/L) \\ &= o(1/L) \end{aligned}$$

From this asymptotic work taking terms of size $O(1)$, we consider far simpler acceleration equations for our analytic work, namely

$$\ddot{x} = \frac{\beta}{h} \left(\frac{1}{x} + \frac{1}{x-1} \right) \quad (5)$$

and

$$\ddot{y} = 0. \quad (6)$$

This nearly constant y -velocity as mentioned in the numerical results is expressed by the zero y -acceleration.

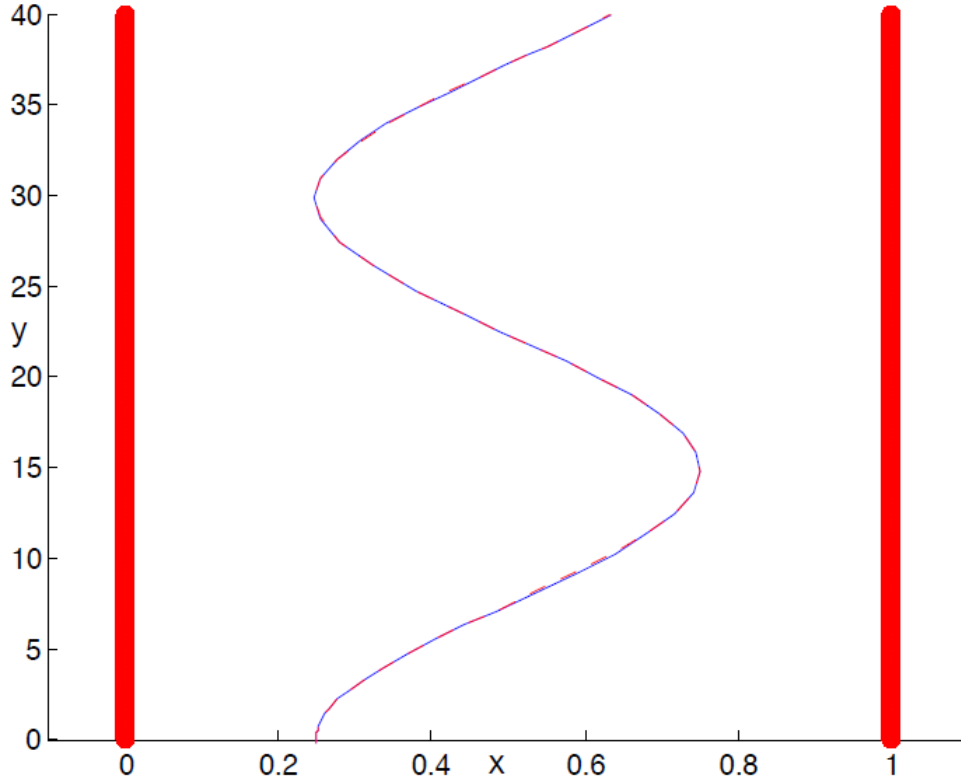


Figure 7: The trajectories of a single mass m with the blue solid curve representing the trajectory for the full summation model (1) and the red dashed curve representing the trajectory for the model (3) with the summations replaced by integrals.

If we consider (5) a final simplification of our whole model then we can actually use it to approximate the period of oscillation. Firstly, we can multiply (5) by \dot{x} and integrate to get

$$\dot{x} = \pm \sqrt{\frac{2\beta}{h}} \log \left(\frac{x(x-1)}{x_0(1-x_0)} \right)$$

where the change in sign comes from the transition through turning points in the oscillation. Note that this model is only valid near the middle of the device and this x_0 value is the initial position away from equilibrium for the trajectory in this asymptotic regime where $x_0 < 1/2$ and $\dot{x} = 0$ when $x = x_0$; it isn't necessarily the same as the x_0 value in the initializations for the numerics. If we integrate this expression once more from the initial time $t = 0$ where $x = x_0$ to the turning time $t = T_{1/2}$ where $x = 1 - x_0$ then we recover the half-period,

$$T_{1/2} = \sqrt{\frac{2h}{\beta}} I(x_0)$$

where

$$I(x_0) = \int_{1/2}^{1-x_0} \frac{dx}{\sqrt{\log(x(1-x)) - \log(x_0(1-x_0))}}.$$

Here we integrate only from the equilibrium position by exploiting an even symmetry in the integral. Given a fixed initial position, $I(x_0)$ can be computed numerically. The integral is singular but integrable. If all parameters are fixed aside from mass then since β depends inversely on mass we have a dispersion relation,

$$T_{1/2} \propto \sqrt{m}. \quad (7)$$

We plot the full period ($T = 2T_{1/2}$) dispersion relation in Figure 8 with the parameters taken from Table 1 and the simulations in section 3.

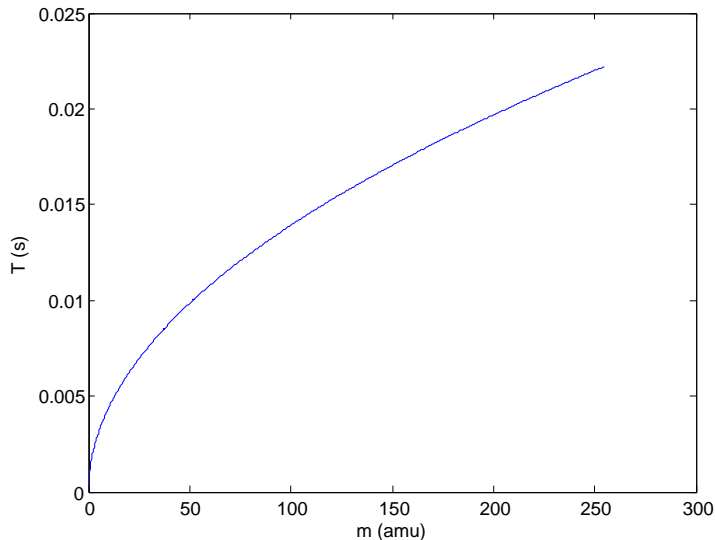


Figure 8: Dispersion relation of the period T versus the mass m . This figure is in dimensional units with m in atomic mass units and T in seconds.

Finally, in Figure 9, we plot the $x(t)$ solution (in blue solid) from the full numeric simulation of (1) along with the solution $x(t)$ (in red dashed) from (5). The approximation of the integral model ignores the portion of the time spent outside the device and this has the effect of inducing a phase difference between the predicted and numerical solutions.

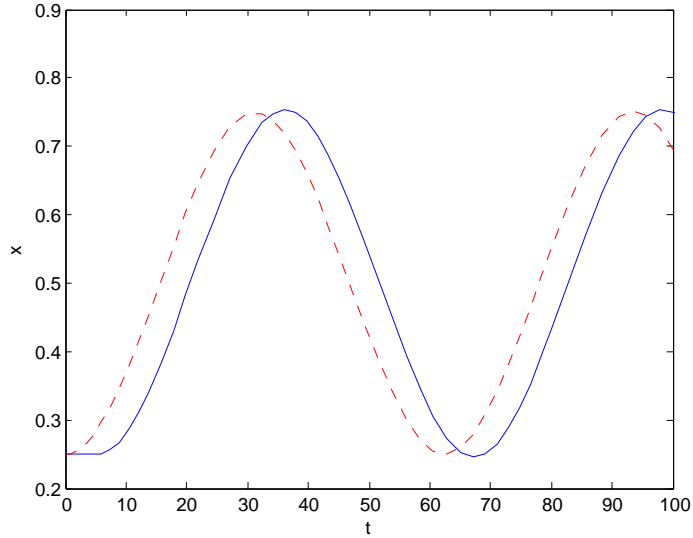


Figure 9: The full numerical solution to (1) plotted in a blue solid curve along with the full numerical solution to (5) plotted in a red dashed curve. This figure demonstrates the synchronous period between the two models.

The period approximation (7) is the exact period for the red dashed solution and an approximation to the full period. Indeed, the figure shows the agreement between the periods of the two models. The phase difference results from model equation (5) approximating the system with the mass already inside a one-dimensional oscillator while the full model has a lag as the mass enters the device.

5 Conclusions and Future Work

We have designed a device that separates components of a chemical substance by mass and detects them simultaneously, thus addressing the problem that was proposed by the industrial partner. Our device solely uses an electric field and does not trap the ions as they travel thus being considerate of both the financial and physical constraints stipulated by the sponsoring company. While the full model is relatively intractable to analytic analysis, we have demonstrated that with some very insightful simplifications, we can recover a mass-dispersion relation for any sample. While actual device imperfections make this curve a theoretical one, it could still serve as a benchmark for calibrating any machine made using this technology.

Possibly by combining a solenoidal design with more complicated engineering practices, such as a length-dependent potential or variable coil radius, the desired effects could be produced.

We decided to not focus on the feasibility of particle detection when considering our model as this is an entirely different engineering problem. Here we propose two methods

that could be useful in detecting different types of particles. Firstly, we consider that an areal detector could be placed along the device. Since the particles travel along different trajectories, they would cross an areal detector at different positions in the plane of the detector. Using data fitting to the curve generated in Figure 8, one could calibrate the device based on certain control masses. A second detection mechanism could involve the ability to measure the oscillating signal of the masses. Through Fourier techniques, the oscillations could be decomposed and the mass constituents identified.

6 Competing Interests

The authors declare they have no competing interests.

7 Authors' Contributions

This paper was written and edited by ML and IM. Mathematical analysis of the models, numerical simulations of the trajectories, and force interaction simulations were done by ML and IM. Parts of the particle-particle force interaction code were provided by KR. ML, IM, and KR compiled references. All authors read and approved the final manuscript.

8 Acknowledgments

The authors would like to thank the Fields Institute for hosting the 2014 Fields-MPrime Industrial Problem Solving Workshop that provided us the venue and opportunity for this work and for paying for our travel expenses and accommodations. The authors also wish to thank Jeremy Budd and Mary Pugh for their involvement in the group work at the workshop, and Samad Bazargan of PerkinElmer for presenting this very interesting problem.

References

- [1] I Jonathan Amster et al. Fourier transform mass spectrometry. *Journal of mass spectrometry*, 31(12):1325–1337, 1996.
- [2] Igor V Chernushevich, Alexander V Loboda, and Bruce A Thomson. An introduction to quadrupole–time-of-flight mass spectrometry. *Journal of Mass Spectrometry*, 36(8):849–865, 2001.
- [3] David Jeffrey Griffiths and Reed College. *Introduction to electrodynamics*, volume 3. Prentice hall Upper Saddle River, NJ, 1999.
- [4] Christine M Mahoney. *Cluster Secondary Ion Mass Spectrometry: Principles and Applications*, volume 44. John Wiley & Sons, 2013.

- [5] Philip E Miller and M Bonner Denton. The quadrupole mass filter: basic operating concepts. *Journal of chemical education*, 63(7):617, 1986.